Published by Avanti Publishers

International Journal of Petroleum Technology

ISSN (online): 2409-787X

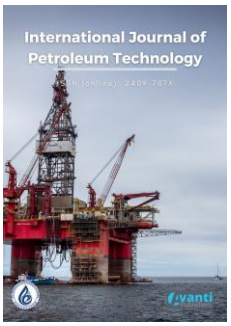

Research on the Method of Evaluating the Pore Throat Structure of Rock Microscopically Based on the 3D Pore Network Model of Digital Core

Ganggang Yan*, Wende Yan, Yingzhong Yuan, Xiujun Gong, Ziqi Tang and Bai Xueyuan

Chongqing Key Laboratory of Complex Oil & Gas Fields Exploration and Development, Chongqing University of Science & Technology, Chongqing 401331, China

ARTICLE INFO

Article Type: Research Article

Keywords:
Pore microstructure
Pore network model
Petroleum engineering
Oil-water two-phase flow
Low permeability fractured reservoir parameters Digital core

Timeline:
Received: September 19, 2022
Accepted: October 14, 2022
Published: December 5, 2022

Citation: Yan G, Yan W, Yuan Y, Gong X, Tang Z, Xueyuan B. Research on the method of evaluating the pore throat structure of rock microscopically based on the 3D pore network model of digital core. Int J Petrol Technol. 2022; 9: 44-53.

DOI: https://doi.org/10.54653/2409-787X.2022.09.6

ABSTRACT

In order to solve the problems of time-consuming, poor repeatability and inability to directly reflect the pore structure of the core by traditional experimental methods to obtain the reservoir parameters, a method was proposed to study the pore structure of inner core using digital core and pore network model. Firstly, the core CT scan image is processed by filtering and denoising, threshold segmentation and pore-throat network skeleton extraction. Then, the digital core and pore network model are constructed by digital image technology and maximum sphere algorithm, and the core physical parameters are statistically analyzed. Finally, a digital core pore network model is used to simulate oil-water two-phase flow. The results show that the digital core pore network model can better reflect the real core pore space characteristics and accurately reflect the pore throat distribution and morphology characteristics. Through practical application, the 3D pore network model of a digital core can accurately reflect the core's microporosity and throat structure and fully understand the mechanism of fluid flow in porous media, which has high application value. In addition, the method can be repeated many times, which is time-consuming and controllable and makes up for the limitations of conventional physical experiments.

*Corresponding Author
Email: 15774630787@163.com
Tel: +(15) 025869381

1. Introduction

With the rapid development of computer computing power, digital core technology has been widely used in developing oil and gas fields. A series of achievements have been made in the microscopic study of rock physics in complex reservoirs. The digital core technology is an emerging means to analyze the macroscopic physical properties of rock from the microscopic scale based on core structure information. It studies the microscopic structure of rock through mathematical modeling, quantitative analysis, and physical field simulation. To reflect the pore structure of rock and quantitatively study the influence of various microscopic factors on the physical properties of rock [1, 2]. Through systematic investigation, the commonly used methods for digital cores can be divided into three categories: numerical reconstruction method, physical experiment method, and hybrid method combining Simulated annealing method and position-based model [3–7]. Digital cores can better reflect the pore space characteristics of real cores and accurately reflect the spatial distribution and morphology characteristics of real cores. The application of digital core technology can not only quantitatively characterize the micro-pore structure of the core but also simulate the micro-seepage of a core with simulation software, guiding oilfield development.

The digital core is an important technique for solving rock physics problems. The traditional experimental methods can only study the flow state of low permeability fractured reservoir from the macroscopic perspective. However, they cannot study the pore structure of rock from the microscopic perspective. Digital cores can not only explain macroscopic phenomena from a microscopic perspective but also better reflect the pore space characteristics of real cores and more accurately reflect the spatial distribution and morphological characteristics of real cores [8–11]. The digital core pore network model has become an essential tool to characterize the microscopic pore structure of rock since it was introduced into the field of rock analysis [7, 12, 13]. In the past, pore network models are mainly used to study the microscopic pore structure of rock, but few studies on low permeability fracture-pore dual media. Therefore, based on CT scan core images, this study adopts digital core modeling technology to establish a 3D digital core model and uses the maximum sphere method to extract the real fracture-pore network model respectively. Finally, the porosity and permeability of rock samples were calculated based on the constructed fracture-pore network model and compared with the conventional physical property experimental data to verify the model's reliability.

2. Rock CT Scan Experiment

To test the reliability of the fracture-pore network model building method of double type selection of LN10 oilfield fracture-pore carbonate rock samples (Fig. **1a**), the dual network model calculated will be based on the pore-fracture porosity and permeability, absolutely and conventional petrophysical experiment concluded that the porosity and absolute permeability were compared. Firstly, the samples were scanned by CT respectively, with a scanning accuracy of 30mm and a view range of 10mm×10mm×10mm. A total of 1000 two-dimensional gray projection images were obtained by CT scanning gray images (Fig. **1b** and Fig. **1c**). Through gray image rendering and local amplification. It can be that the pores inside the sample are all developed (Fig. **1d**). The scanning parameters were as follows: voltage 110kV, current 100μA, the scanning mode was step-scan, each rotation was 0.225, the exposure time was 1500ms, the image size was 3052 pixel × 2400 pixel, sample scanning resolution was 10μm/pixel.

3. Construction of Low Permeability Fracture Pore Three-Dimensional Model

Grayscale images obtained by CT scanning are combined with image processing technology and digital core technology to reconstruct 3D core images and extract pores. Firstly, the CT scanning method obtained grayscale images of pore-fracture carbonate samples for denoising and binarization. Then, constructing a chain to do the Monte Carlo approximation method is used to reconstruct the skeleton and pore structure of the segmented image. Finally, image segmentation technology separates the pores in the image from the rock skeleton, and a 3D pore network model of the digital core is established.

(**a**) Core sample

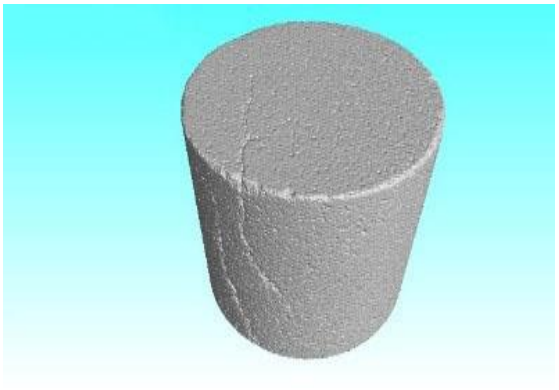

(**b**) Core CT scan 3D image

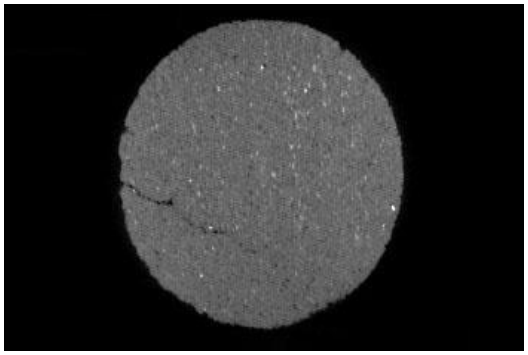

(**c**) Projection cross-section of core CT scan

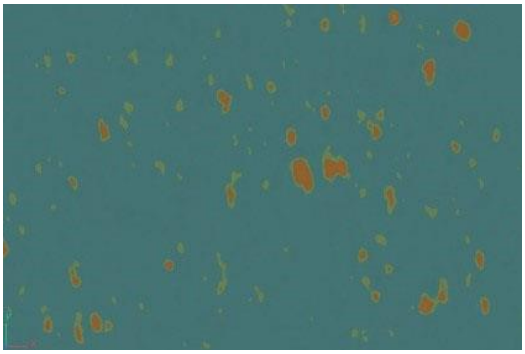

(**d**) Partial enlargement (rendering)

Figure 1: Grayscale image of sandstone CT scan.

3.1. Binarization Processing of Rock Sample Image

In the process of CT core scanning, it will be affected by some signal noise and other factors, so the gray image after Reconstruction does not reflect the core image. Therefore, the median filtering method is used to remove the noise. The median filtering method is simple and can maintain the image edge well, which is very suitable for core CT image denoising and filtering. The filtered structure is shown in Fig. (**2a**) below. The CT image after median filtering is a mixture of pores and rock skeletons with different gray levels. In order to distinguish rock skeleton and pore, it is necessary to perform binarization processing on the CT scan image of the rock. The maximum between-group variance method is used to segment the core image's pore and skeleton, which has good adaptability and stability. In addition, compared with other methods, the maximum between-group variance method can take advantage of the different gray values of pores and skeletons in core slice images. The image is divided into two parts, background, and target. If the inter-class variance between the two parts is more significant, the difference between the two parts is more obvious. Therefore, using the maximum between-group variance method to segment, the slice image can reduce the error rate and improve the accuracy of the digital core model. The core image segmentation results are shown in Fig. (**2b**).

3.2. 3D Fracture Pore Network Model Construction

The pore and skeleton in the image are distinguished by pre-processing the 2d core slices with noise reduction and binary segmentation. In order to meet the needs of pore structure characteristics of the sample core, the pore network is extracted from the pore space of the digital core by the maximum ball filling method. Based on any voxel in the segment pore space, the expansion algorithm determines the possible search space and the closest range of skeleton voxel for each voxel. The contraction algorithm is used to identify the end-tangent sphere corresponding to the central voxel, and the upper and lower limits of the end-tangent sphere radius are calculated. Because the pore structure inside the core is too complex, it is necessary to simplify the core and extract the pore throat with a simple shape, the same flapping structure, and equivalent.

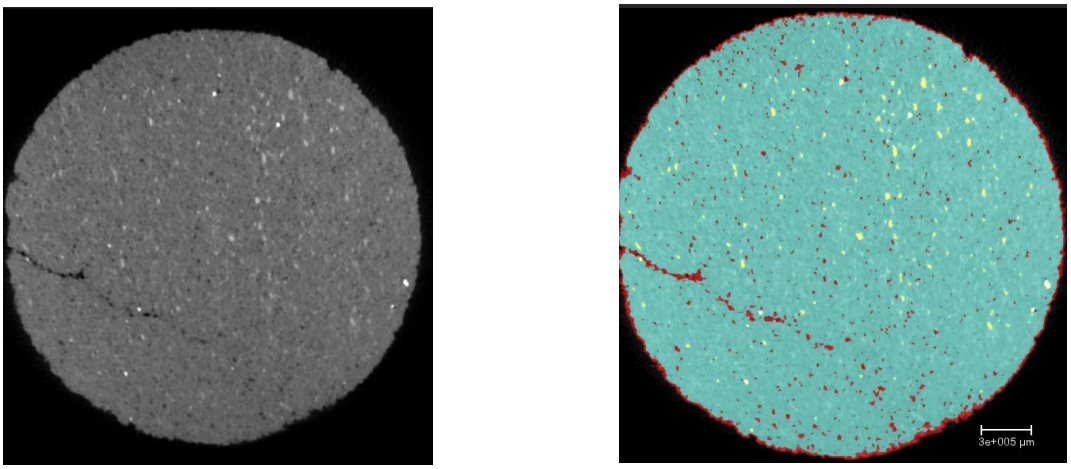

(**a**) Image of the filtered rock sample (**b**) Image of segmented rock sample

Figure 2: Pores obtained from gray image segmentation of CT scan of rock sample.

Irregular pore and throat Spaces are described by regular geometry. The new graph generated after translation, scaling, and rotation transformation is used to verify the geometric transformation technology by cutting the core graph. The pore point (central axis node) is selected to be large enough. Using graph transformation, the neighborhood is dissected at a series of evenly spaced angles to obtain pore profiles in different directions. Taking the pore point as the origin, a ray is emitted at a certain Angle in the section plane. When the ray is extended to the rock particles, the growth of the ray stops, and the length of all ray segments is recorded until all sections are processed. The maximum interclass variance method was used to process the data set composed of ray segment length values obtained in the above process. The optimal separation threshold, namely, porosity length, was obtained. The pore length is taken as the radius to make the sphere, the voxel points in the pore sphere are the pore points contained in the largest sphere, and statistical voxel points obtain the pore volume. Using the maximum sphere method and the above steps, pore network models corresponding to each digital core are established based on digital cores, as shown in Fig. (**3**). As can be seen from the figure, the pore size distribution of the core is relatively uniform, with good homogeneity and pore connectivity.

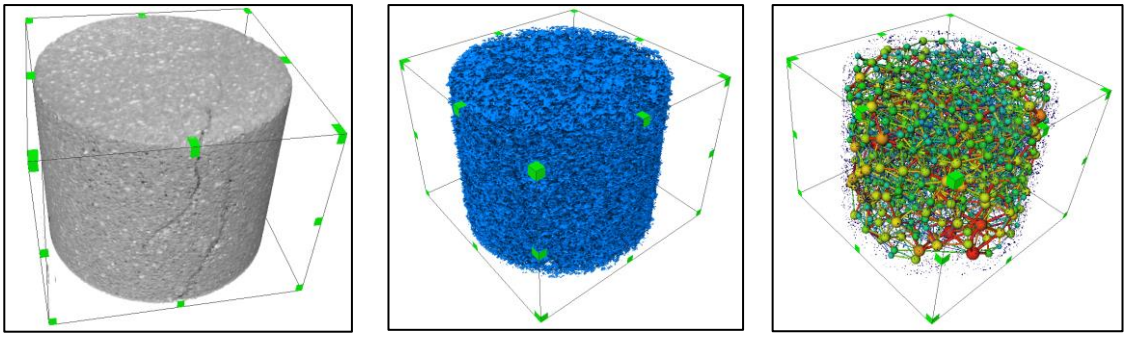

(**a**) Digital core 3D model (**b**) Fracture-pore network model (**c**) Bats model

Figure 3: Digital core fissure-pore network model.

The distribution of the pore coordination number reflects the connectivity of the pore network model. The larger the peak value of pore coordination number distribution is, the better the connectivity. The pore space topological structure was studied by statistical analysis of the pore coordination number distribution of the pore network model. The pore coordination number distribution of the rock sample is shown in Table **1** and Fig. (**4**) below. It can be seen from Fig. (**4**) that the pore coordination number distribution of the rock sample presents a single-peak distribution, mainly concentrated in 0~5, indicating that the pore connectivity of the rock sample is poor.

Table 1: Statistical table of pore coordination number of rock sample.

Name	Maximum	Minimum	Average
The pore coordination number of rock sample	25	0	2.72866

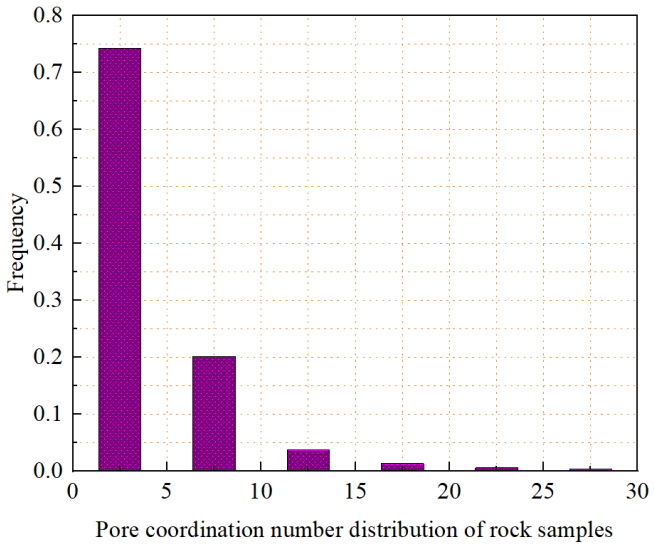

Figure 4: Pore coordination number distribution of rock samples.

4. Calculation of Model Petrophysical Parameters

4.1. Calculation of Porosity of Pore Network Model

The spatial structure of the pores is very complex, and the length of the pores is different in different directions. Therefore, the partition threshold is introduced to calculate the pore length based on maximum interclass variance. Firstly, the maximum sphere method is used to obtain the pore radius, the pore point is used as the center of the sphere to make the sphere, and the infinite approximation method is used to increase the sphere's radius until the sphere contacts the skeleton voxel point. At the time, the sphere is the maximum end-tangent sphere of the pore, and the radius of the maximum end-tangent sphere is the pore radius. Then use image transformation from a different point of view of porosity in different directions cutting plane, pore as the origin, the cutting plane inside a ray from every Angle, when the rays extended to rock particles stop extending, the use of the between-cluster variance with a length of a ray is composed of data collection, get the between-cluster variance, the pore length. It is shown in Fig. (**5**) below.

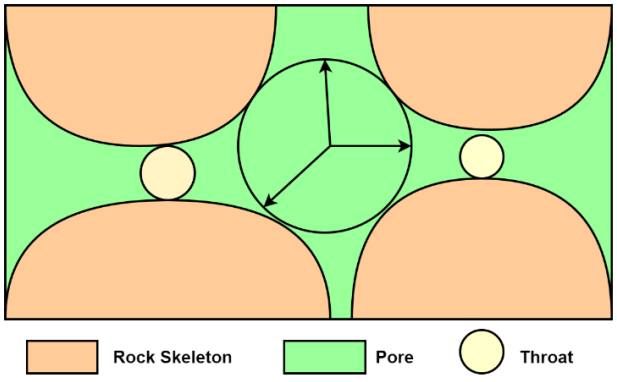

Figure 5: Schematic diagram of pore and throat simplified by the maximum spherical method.

The porosity of the pore-fracture dual network model can be obtained by calculating the percentage of the sum of pore space volume and fracture space volume and the total volume of the sample [14]:

$$\emptyset = \frac{V_p + V_f}{V_b} \times 100\% \tag{1}$$

ϕ—Porosity, %; Vp–Pore-space volume, μm^3; V_b–Fracture space volume, μm^3; V_b–Sample volume, μm^3。

4.2. Calculation of Permeability of Pore Network Model

The pore-fracture dual network model is a quasi-static model in which capillary forces control all fluid flows. When calculating the absolute permeability, it is assumed that the throat is saturated with fluid. The driving pressure p_i and p_j are applied at both ends of the throat between the interconnected pore i and pore j. The relationship between the flow rate and pressure drop is as follows [15]:

$$q_{ij} = g_{ij}(p_i - p_j) \tag{2}$$

q_{ij}–The flow of fluid in pore i into pore j, cm^3/s; p_i–Pore i end pressure, atm; p_i–Pore j-end pressure, atm; g_{ij}–Conductivity of the throat connecting pore i to pore j, $cm^3/\ (atm \cdot s)$.

According to Poiseuille's law, the conductivity g_{ij} is:

$$g_{ij} = \frac{\pi r^4}{8\mu l} \tag{3}$$

r–Throat radius, cm; μ–v, $mPa \cdot s$; l–length of the throat, cm。

For the steady flow of incompressible fluid, the flow into each pore in the model should be equal to the flow out, so the mass conservation of each pore can be expressed as:

$$\sum_{i \to j} q_{ij} = 0 \tag{4}$$

By solving equations (2) - (4) simultaneously, the pressure of each pore can be obtained, which can be applied to all pores, and the total flow Q under pressure difference at both ends of the model can be further calculated. According to the Darcy formula, the absolute permeability of the pore-fracture dual network model can be calculated:

$$K = \frac{Q\mu L}{(p_i - p_j)A} \times 10^8 \tag{5}$$

K–Permeability, D; Q–Total fluid flow in the modelcm^3/s; L–Length of the model, cm; A–Pore and throat sections, cm^2。

4.3. Calculation of Pore Factor and Throat Shape Factor

The pore shape factor is an important parameter to characterize pore shape, and the throat radius is an important parameter to calculate the critical seepage pressure of fluid flowing through the throat. Due to the complex shape of the pores and throats in real cores, the pores and throats are reduced to simple, uniform sections.

In order to improve the accuracy of the model, it is necessary to quantitatively characterize the shape characteristics of core pores and throats, so the shape factor is introduced [16–20]:

$$S_f = \frac{A}{L^2} \tag{6}$$

S_f–Shape factor; A–Pore and throat cross-section area, cm^2; L–The circumference of the shape of the pore and throat section, cm。

By modeling the digital core and optimizing the pore space, the topology of the pore space of the digital core is obtained. By using the processed images, using the maximum sphere method and three-dimensional geometric transformation technology, the pore and throat are identified, the pore and throat positions are obtained, and the geometric parameters of each pore and throat are calculated, such as pore radius, pore shape factor, throat radius, and throat shape factor, etc.

5. Case Analysis

After the pore space is separated from the reconstructed digital core model, the ball-and-stick model of the pore system is established using the pore network model obtained above. This model can not only express the distribution characteristics of pore throat intuitively but also quantitatively describe the distribution characteristics of the pore through quantitative measurement and statistics of "sphere," that is, statistical analysis of pore distribution characteristics in the sample. In order to facilitate the analysis of the properties of each pore network model, Origin software was used for statistical analysis of pore radius, pore shape factor, throat radius, and throat shape factor. The statistics of each parameter are shown in Table **2**.

Table 2: Parameters calculated by the pore network model.

Model Name		Sample			
Model Size (voxel × voxel × voxel)		$10 \times 10 \times 10$			
Porosity (%)		5.91			
The total number of pores		84252			
The total number of shouted		57114			
Pore Radius /μm	Maximum	2.67047	Pore Shape Factor	Maximum	0.06406
	Minimum	0.10165		Minimum	0.00505
	Average	0.86972		Average	0.04216
Shouted Radius /μm	Maximum	2.11213	Roared Shape Factor	Maximum	0.07506
	Minimum	0.09657		Minimum	0.00191
	Average	0.6284		Average	0.02336

Pore throat size mainly refers to the radius of the pore and throat. Throat radius, a basic structural parameter in porous reservoir media, is also the key to constructing a digital pore model. The throat radius determines the resistance calculation and fluid's spatial distribution during fluid displacement. The pore radius, throat radius, pore shape factor, and throat shape factor of cores with different numbers were counted, and their distribution was shown in Fig. (**6**).

In order to deeply analyze pore structure and pore size distribution, statistical analysis was carried out from two aspects of pore throat radius and pore throat shape factor according to the three-dimensional pore network model. As can be seen from the relevant data of pore and throat radius in Table **2** and Fig. (**6**). The core's pore radius and throat radius show a single-peak distribution trend of high in the middle and low on both sides. The pore radius is mainly concentrated around 0.75um, and the throat radius is mainly concentrated around 0.65um. The pore radius and throat radius are more concentrated, indicating that the pore space distribution is homogeneous, the pore space is mostly uniform, and the homogeneity is substantial.

In order to simplify the problem, the complex pores and throats in real cores are characterized by the regular assembly. The simplification process follows the principle of shape factor conservation, and the statistical results of the shape factor of the digital sandstone core are shown in the figure. As seen from Fig. (**7**), the distribution of

the pore shape factor and throat pore factor of different cores shows a single-peak distribution trend, with the pore shape factor around 0.375 and the throat shape factor around 0.012.

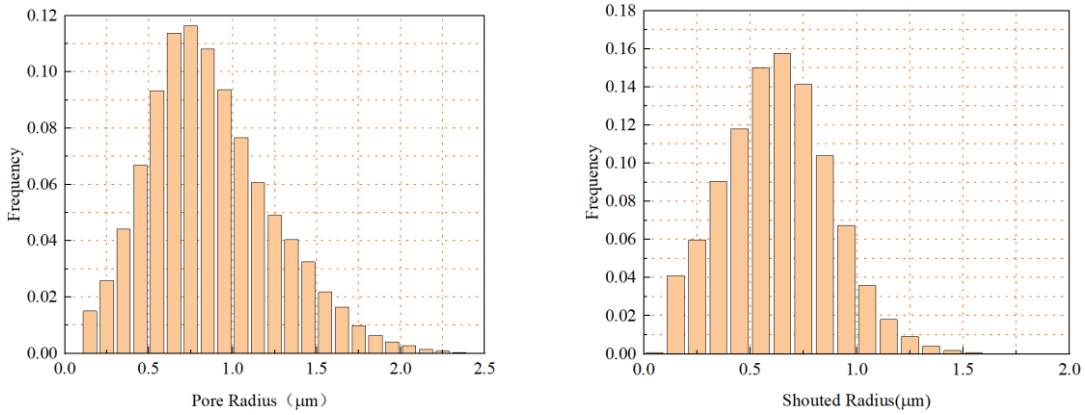

Figure 6: Distribution of pore radius and pore throat radius of digital core.

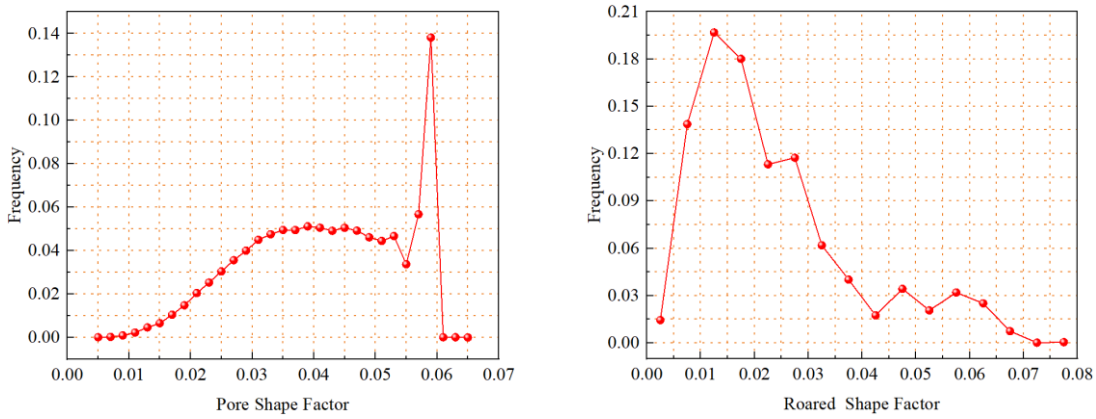

Figure 7: Distribution of digital core pore factor and throat factor.

The porosity and permeability values calculated by the digital core pore network model are compared with those measured in the laboratory, as shown in Table **3** below.

Table 3: Core porosity and permeability [21].

Name	Porosity (%)	Permeability(mD)
Laboratory measurement	6.41	0.45
Other laboratory measurements	8.3	1.44
Numerical core pore network model calculation	5.91	0.86

In conclusion, there is a good consistency between the results measured in the laboratory and those measured in the pore network of digital cores. Therefore, the quantitative characterization results of pores obtained by the pore network model reconstructed by the digital core technology through CT scanning cores are reliable.

6. Conclusion

Through noise reduction, filtering, and threshold segmentation of CT scan rock gray image, rock physical properties are simulated based on processed digital core data, and a 3D pore network model reflecting the real microstructure of the core is constructed by digital core. Based on the network model, the pore throat size, pore

space topology, and pore throat shape characteristics in each pore network model are compared and analyzed. The results show that:

(1) CT scan can accurately identify pore throats with diameters larger than 12.40μm in samples with diameters of 2.5cm and height of 5cm and display the distribution of pore throats in three-dimensional space. The pore throat radius distribution trend in the core is positive, so the pore throat distribution has significant homogeneity.

(2) The core pore shape factor and throat shape factor presents a single-peak distribution, with peak values around 0.375 and 0.012, respectively. The core throat shape factor distribution mainly concentrates on the right side of 0.012, indicating that the pores developed in the core are relatively round. The core shape factor is relatively small, and the pore and throat corner structure is relatively obvious.

(3) The porosity and permeability measured in the laboratory and the porosity and permeability measured by the digital core pore network model have an error of 3%. Therefore, the quantitative characterization results measured by the three-dimensional pore network model are more reliable. CT scanning technology can realize the visualization characterization of micro-pore structures at different scales, which provides conditions for the study of pore networks in porous media and the construction of digital cores.

There are two future directions. First, we only implemented two-level matching, but the approach should be generalized to multiple scales, for example, to connect centimeter-millimeter-micron-nanometer scales. Second, template matching with 3D templates, while computationally much more expensive to implement (correlations must be computed in three directions and two angular rotations), should be more accurate at recognizing microstructure but might also require fewer templates.

Acknowledgement

Science and Technology Research Project of Chongqing Education Committee “Research on hydration mechanism of shale reservoir-fracturing fluid and gas-water two-phase seepage model” (KJQN202001501).

Science and Technology Innovation Research Project of Chongqing University of Science &Technology Chongqing “Research on Digital Core Modeling and Pore Network Simulation of Low Permeability Fractured Reservoir” (YKJCX2120106).

References

[1] Hai-Tao W, Li W, Fu-Qiang L, Jin-Yan Z. Investigation of image segmentation effect on the accuracy of reconstructed digital core models of coquina carbonate. App Geophys. 2020; 17: 501-12. https://doi.org/10.1007/s11770-020-0846-2.

[2] Zhao Y, Li X, Fang Z, Yong’an Z, Mingke Z, Xing D. Numerical simulation of resistivity of 3D digital core of fractured shale oil reservoir. J Xi’an Shiyou Univ Nat Sci Ed. 2022; 37: 51-7. https://doi.org/10.3969/j.issn.1673-064X.2022.01.006.

[3] Li Q, Chen Z, He J-J, Hao S-Y, Wang R, Yang H-T, *et al*. Reconstructing the 3D digital core with a fully convolutional neural network. App Geophys. 2020; 17: 401-10. https://doi.org/10.1007/s11770-020-0822-x.

[4] Cui L-K, Sun J-M, Yan W-C, Dong H-M. Multi-scale and multi-component digital core construction and elastic property simulation. App Geophys. 2020; 17: 26-36. https://doi.org/10.1007/s11770-019-0789-7.

[5] Mosser L, Dubrule O, Blunt MJ. Stochastic reconstruction of an oolitic limestone by generative adversarial networks. Transp Porous Media 2017; 125: 81-103. https://doi.org/10.1007/s11242-018-1039-9.

[6] Altowairqi Y, Rezaee R, Urosevic M, Piane CD. Measuring ultrasonic characterisation to determine the impact of TOC and the stress field on shale gas anisotropy. APPEA J. 2013; 53: 245-54. https://doi.org/10.1071/AJ12021.

[7] Long J, Shelhamer E, Darrell T. Fully convolutional networks for semantic segmentation. 2015 IEEE Conference on Computer Vision and Pattern Recognition (CVPR), vol. 39, IEEE; 2015; p. 3431-40. https://doi.org/10.1109/CVPR.2015.7298965.

[8] Xiao X, Zhang X, Zhang J, Luo X. Study of three-dimensional digital core reconstruction based on multiple-point geostatistics in a cylindrical coordinate system. IEEE Access 2019; 7: 8522-7. https://doi.org/10.1109/ACCESS.2019.2957580.

[9] Arns CH, Bauget F, Sakellariou A, Senden TJ, Sheppard AP, Sok RM, *et al*. Digital core laboratory: petrophysical analysis from 3D imaging of reservoir core fragments. Petrophysics 2005; 46: 122-34.

[10] Zhou S, Yan G, Xue H, Guo W, Li X. 2D and 3D nanopore characterization of gas shale in Longmaxi formation based on FIB-SEM. Mar Pet Geol. 2016; 73: 174-80. https://doi.org/10.1016/j.marpetgeo.2016.02.033.

[11] Wu Y, Lin C, Ren L, Yan W, An S, Chen B, *et al*. Reconstruction of 3D porous media using multiple-point statistics based on a 3D training image. J Nat Gas Sci Eng. 2018; 51: 29-140. https://doi.org/10.1016/j.jngse.2017.12.032.

[12] Gubaidullin MG, Belozerov IP. Digital core modeling technology for determining the reservoir-capacitive properties of terrigenous reservoirs. IOP Conf Ser Mater Sci Eng. 2021; 1201: 60-73. https://doi.org/10.1088/1757-899X/1201/1/012065.

[13] Mahendran S, Ali H, Vidal R. 3D pose regression using convolutional neural networks: IEEE conference on computer vision and pattern recognition workshops (CVPRW)., IEEE; 2017, p. 2174-82. https://doi.org/10.1109/CVPRW.2017.73.

[14] Wang Y, Arns CH, Rahman SS, Arns J-Y. Porous structure reconstruction using convolutional neural networks. Math Geosci 2018; 50: 781-99. https://doi.org/10.1007/s11004-018-9743-0.

[15] Li Q, Chen Z, He J-J, Hao S-Y, Wang R, Yang H-T, *et al*. Reconstructing the 3D digital core with a fully convolutional neural network. App Geophys. 2021; 17: 401-10. https://doi.org/10.1007/s11770-020-0822-x.

[16] Hasnan HK, Sheppard A, Hassan MHA, Abdullah WH. Digital core analysis: Characterizing reservoir quality through thin sandstone layers in heterolithic rocks. J Appl Geophy. 2020; 182: 104-15. https://doi.org/10.1016/j.jappgeo.2020.104178.

[17] Wu Y, Lin C, Ren L, Yan W, An S, Chen B, *et al*. Reconstruction of 3D porous media using multiple-point statistics based on a 3D training image. J Nat Gas Sci Eng. 2019; 51: 129-40. https://doi.org/10.1016/j.jngse.2017.12.032.

[18] Aghaei A, Piri M. Direct pore-to-core up-scaling of displacement processes: Dynamic pore network modeling and experimentation. J Hydrol (Amst.) 2015; 522: 488-509. https://doi.org/10.1016/j.jhydrol.2015.01.004.

[19] Madonna C, Quintal B, Frehner M, Almqvist BSG, Pistone M, Marone F, *et al*. Synchrotron-based X-ray tomographic microscopy for rock physics investigations. Geophysics 2020; 78: 53-64. https://doi.org/10.1190/GEO2012-0113.1.

[20] Gubaidullin MG, Belozerov I.P. Digital core modeling technology for determining the reservoir-capacitive properties of terrigenous reservoirs. IOP Conf Ser Mater Sci Eng. 2021; 1201: 012065-63. https://doi.org/10.1088/1757-899X/1201/1/012065.

[21] Zhu W. Study on digital rock reconstruction using the process-based method. Prog Geophys. 2020; 35: 1539-44. https://doi.org/10.6038/pg2020DD0232.